INTERNATIONAL JOURNAL OF HYDROGEN ENERGY XXX (2017) 1–12

Available online at www.sciencedirect.com

ScienceDirect

journal homepage: www.elsevier.com/locate/he

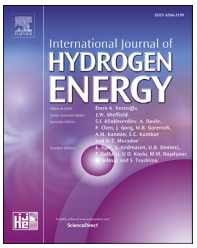

Well-dispersed Rh nanoparticles with high activity for the dry reforming of methane

Betina Faroldi [a], *John Múnera* [a], *Juan Manuel Falivene* [a], *Inmaculada Rodríguez Ramos* [b], *Álvaro Gutiérrez García* [c], *Loreto Tejedor Fernández* [c], *Silvia González Carrazán* [c], *Laura Cornaglia* [a,*]

[a] *Instituto de Investigaciones en Catálisis y Petroquímica, INCAPE, Universidad Nacional en Litoral, CONICET, Facultad de Ingeniería Química, Santiago del Estero, 2829-3000 Santa Fe, Argentina*

[b] *Instituto de Catálisis y Petroleoquímica, CSIC, Marie Curie 2, L10, 28049 Madrid, Spain*

[c] *Departamento de Química Inorgánica, Facultad de Ciencias Químicas (Universidad de Salamanca), Plaza La Merced s/n, 37008 Salamanca, Spain*

ARTICLE INFO

Article history:
Received 27 December 2016
Received in revised form
1 April 2017
Accepted 10 April 2017
Available online xxx

Keywords:
Dry reforming
Rh nanoparticles
SiO_2 binary supports
Pure hydrogen
Membrane reactor

ABSTRACT

Rh catalysts with low Rh content were prepared by incipient wetness impregnation using $[NH_4]_3[RhCl_6]\cdot 3H_2O$ or $RhCl_3\cdot 3H_2O$ as precursor salts, on $CaO{-}SiO_2$ supports. All solids showed a high stability after 48 h on stream for the dry reforming of methane with low carbon content, which made them suitable for obtaining ultrapure hydrogen in a membrane reactor. The methane conversion and hydrogen recovery were measured increasing the sweep gas flow rates to rise the driving force for hydrogen permeation. The catalyst with 0.36 wt.% of Rh showed a slight deactivation. However, the Rh(0.6)/$CaO{-}SiO_2$ solid, in which the Rh impregnation was performed using $[NH_4]_3[RhCl_6]\cdot 3H_2O$, exhibited an increase on CH_4 conversion of 77% and a hydrogen recovery equal to 84%.

Nanoparticles of about 1.4–1.7 nm surface average diameter were detected for the reduced and used solids indicating that Rh is well dispersed and sintering was not produced after the catalytic tests. Rh particle sizes calculated by CO chemisorption were coincident with those measured by Transmission Electron Microscopy. Characterization by this technique and Laser Raman Spectroscopy of the solids used in membrane reactor revealed the formation of scarce carbon filaments. However, a surface re-oxidation was detected in the low loading catalyst used in the membrane reactor suggesting that it is the main cause for the decrease in the activity of the highly dispersed catalyst.

Introduction

The production of synthesis gas from the dry reforming of methane (DRM) is becoming an attractive topic due to the chemical utilization of greenhouse gases such as carbon dioxide and methane. This reaction has a potentially important role in the generation of syngas with H_2/CO ratios more suitable for various oxo-syntheses [1–4]. The practical usefulness of this endothermic reaction could also be improved by combining with an exothermic one such as the partial

* *Corresponding author*. Fax: +54 342 4536861.
E-mail address: lmcornag@fiq.unl.edu.ar (L. Cornaglia).

http://dx.doi.org/10.1016/j.ijhydene.2017.04.070

Please cite this article in press as: Faroldi B, et al., Well-dispersed Rh nanoparticles with high activity for the dry reforming of methane, International Journal of Hydrogen Energy (2017), http://dx.doi.org/10.1016/j.ijhydene.2017.04.070

oxidation of methane [5], frequently called combined reforming of methane (CRM).

In recent years, this reaction has been investigating in membrane reactors using various types of membranes and catalysts to produce high purity hydrogen [5–8]. The proposal of the production and purification of hydrogen by using a membrane reactor has received a great attention in the last decades applying several equilibrium-limited reactions [9–12]. The hydrogen thus obtained would be appropriate for use in fuel cells. The most important factors usually considered that affect the behavior of membrane reactors are percentage of conversion enhancement, H_2 recovery, H_2 purity and catalyst and membrane stability [6,9,13]. On the other hand, catalysts used in the methane reforming reactions can be deactivated due to carbonaceous deposits and/or poisoned with sulfur and other impurities present in the feed. This would be harmful as it would prevent their use in membrane reactors. In addition to catalyst deactivation, carbon deposits could cause the deterioration of the membrane [7].

In the case of dry reforming of methane temperatures above 1023 K and CH_4/CO_2 ratios less than unity should be used to avoid the formation of carbon deposits. However, from an industrial point of view it is desirable to operate at lower temperatures and with CH_4/CO_2 ratios close to unity [14,15]. Therefore, many studies of the CO_2 reforming reaction focus on the development of new catalysts which inhibit the formation of carbon deposits within the operating range where the formation of those deposits are favorable.

The formation of carbonaceous deposits depends on several parameters, such as the metal used as active phase, its crystal structure, metal-support interactions or the basicity of the support. The catalytic activity of various noble and non-noble metals supported on several oxides [1] has demonstrated that most noble metals (Rh, Ru, Pt, etc.) reduce the formation of carbonaceous deposits and show high activity in the reforming reactions but their high cost prevents their use in large-scale applications. Nickel catalysts, conventional catalysts for steam reforming, are more suitable from an economic point of view, however, the major concerns of Ni-based catalysts for DRM include sintering of Ni particles and coke deposition. Both the control of Ni particle size and a proper metal-support interaction may help to prevent Ni sintering and carbon formation [16,17].

The nature of the support affects metal catalytic activity as it modifies the active surface area and the acid–base properties of the catalyst. Since dry reforming involves the adsorption and dissociation of CO_2 acid gas, the catalyst basic character could promote the reaction. For this reason, the addition of alkaline earth oxides such as MgO or CaO over a support such as SiO_2 could prevent the formation of carbon deposits and also hinder the sintering of metal particles [1,15] as we have reported in a previous study of Rh supported on $CaO–SiO_2$ binary systems [18]. The best formula of the binary support, 27 wt.% of CaO on SiO_2, yields the proper interaction with the supported Rh nanoparticles (0.6 wt.%) which would prevent carbon formation.

Therefore, once we found the best composition for the binary support, our next goal was to synthesize catalyst formulations containing less than 0.6 wt.% Rh, which are stable, selective and avoid low carbonaceous deposits. Moreover, the use of very low amounts of Rh would reduce the catalyst cost.

In this work, the surface and structural properties of low loading and well-dispersed Rh catalysts supported on $CaO–SiO_2$, prepared from different chloride-based precursor salts, have been investigated by using X-ray diffraction (XRD), CO chemisorptions, Transmission electron microscopy (TEM), Fourier Transmission Infrared Spectroscopy as well as X-ray photoelectron spectroscopy (XPS). The catalysts, with Rh nanoparticles of about 1.4–1.7 nm, prepared employing $[NH_4]_3[RhCl_6]\cdot 3H_2O$ were the most active, stable ones and free of carbon deposits in the conventional reactor for the dry reforming of methane. To further investigate their catalytic properties, they were also evaluated in a membrane reactor using different operation conditions for the production of ultrapure hydrogen.

Experimental

Preparation of catalysts

SiO_2 (Aerosil 200) previously calcined at 1173 K was employed to synthesize the $CaO–SiO_2$ binary support by incipient wetness impregnation with $Ca(NO_3)_2\cdot 4H_2O$ (Merck). A CaO loading of 27 wt.% was used. After the impregnation, the solid was kept at room temperature for 2 h and then dried in an oven at 353 K overnight. Finally, it was calcined in flowing air at 823 K for 6 h. The metal impregnation (0.36 or 0.6 wt.% of Rh) was performed using $[NH_4]_3[RhCl_6]\cdot 3H_2O$ or $RhCl_3\cdot 3H_2O$ (Alfa Aesar) as precursor salts following the same procedure detailed above.

Samples were denoted as $Rh(X)/CaO–SiO_2$, where X is the wt.% nominal content of Rh. NCl and Cl indicate that $[NH_4]_3[RhCl_6]\cdot 3H_2O$ or $RhCl_3\cdot 3H_2O$ were used as precursor salts.

Characterization techniques

The Brunauer–Emmett–Teller (BET) surface area of the calcined solids was determined using a Micromeritics Gemini VII instrument after degassing during 1 h at 423 K.

The Rh dispersion of the reduced catalysts was determined by static equilibrium of CO adsorption at room temperature in a conventional vacuum system. More details can be found in previous publications [7,18].

The CO adsorption experiments followed by Fourier Transform Infrared Spectroscopy (FTIR) were performed with a Shimadzu spectrometer. The samples were mounted on a transportable infrared cell. After reduction at 823 K, evacuation at 473 K and cooling to 298 K, different CO pressures were admitted. FTIR spectra were recorded following adsorption and evacuation steps at different temperatures [18].

X-ray photoelectron spectroscopy (XPS). A multi-technique system (SPECS) was employed to carry out XPS measurements. All samples were reduced ex situ at 823 K during 2 h. The XPS analyses were performed on the reduced solids after treatment with H_2 at 673 K in the reaction chamber of the spectrometer. All spectra were referenced to the Si 2p binding

Please cite this article in press as: Faroldi B, et al., Well-dispersed Rh nanoparticles with high activity for the dry reforming of methane, International Journal of Hydrogen Energy (2017), http://dx.doi.org/10.1016/j.ijhydene.2017.04.070

energy at 103.5 eV. The data treatment was performed with the Casa XPS program (Casa Software Ltd, UK) [18].

Transmission electron microscopy (TEM) images of the reduced catalysts were acquired using a JEOL 2100F field emission gun electron microscope equipped with an energy dispersive X-ray spectroscopy (EDX) system. The Raman spectra of the used solids were recorded using a LabRam spectrometer (Horiba-Jobin-Yvon). The excitation wavelength was in all cases 532 nm. Each Raman spectrum was collected for ~240 s using a laser power of mW. In order to quantify the carbon deposits, Thermogravimetric analysis (TGA) were performed in a Mettler Toledo TGA/SDTA (Model 851) system.

Catalytic tests

The catalysts were ground and sieved down to 150 μm (100 mesh) prior to be loaded in the tubular quartz reactors. They were heated in flowing Ar and then reduced in H_2 at 823 K for 2 h. After the in situ reduction, the feed gas mixtures were fed to the reactors.

Three different reactor configurations were employed:

i) For the reaction rate measurements, 15 mg of catalyst diluted with 50 mg of inert powder quartz were loaded to the differential reactor (inner diameter, 5 mm). A catalyst mass/total flow ratio (W/F) equal to 4.5×10^{-6} g h ml^{-1} was employed to obtain conversions lower than 10%. From these values, the net and forward reaction rates were calculated to verify differential conditions, as proposed by Iglesia and co-workers [19]. The reactant mixture composition was CO_2:CH_4:Ar = 1:1:1.2 [6,7].

ii) For the equilibrium measurements, the catalysts (200 mg) were loaded into a tubular quartz reactor (inner diameter, 16 mm). For the DRM reaction, the [CH_4:CO_2:Ar] ratios were [1:1:1.2] and [1:1.9:0.3] and when 10% O_2 was fed, the [CH_4:CO_2:O_2:Ar] ratios were [1:1:0.3:0.9] and [1:1.9:0.3:0]. In a previous work [5], we have studied the effect of the oxygen addition on the catalytic behavior of Rh catalysts supported on La based oxides, in which the best result was obtained with 10% O_2 which corresponds to a CH_4/O_2 ratio of 3.3.

iii) The tubular membrane reactor (MR) was built with a commercial dense Pd–Ag alloy membrane (REB Research and Consulting). The catalysts (1.5 g), diluted with quartz chips (2.5 g), were packed in the outer annular region to achieve a membrane area of 8×10^{-4} m^2. For these experiments, a W/F equal to 1.5×10^{-3} g h ml^{-1} was used. Further details have been reported elsewhere [18,20].

In all cases, the reaction temperature was 823 K to preserve the useful life of the Pd based membrane.

Results and discussion

Structural and textural properties

The X-ray Diffraction (XRD) patterns of Rh(X)/CaO–SiO_2 calcined samples (Fig. S1 in Supplementary Information) are similar to those of the SiO_2 support calcined at 1073 K [18]. They show an amorphous pattern and a broadening in the 2θ region between 20° and 35°, which could correspond to the incipient formation of CaO, $CaCO_3$ and/or Ca_2SiO_4. These results suggest that CaO could be highly dispersed in the amorphous silica, which acts as a barrier inhibiting crystallite growth, as reported elsewhere [18].

Fig. 1 shows the adsorption–desorption isotherms of N_2 at 77 K for CaO–SiO_2 support and Rh(X)/CaO–SiO_2 calcined samples. The solids show isotherms of type II according to IUPAC classification [21]. This type of isotherm is characteristic of samples with no pores in which nitrogen condensation occurs. However, they show narrow H3 hysteresis loops which are originated by the adsorption of aggregates of plate-shaped particles forming slit-shaped pores.

The corresponding t-plots can be adjusted to straight lines passing approximately through the origin, and from the slopes of these straight lines, the external surface areas St are calculated (Fig. 2 and Table 1). The differences observed between the values of S_{BET} and St may be considered within the experimental error, given the difficulty of establishing a sufficiently tight extrapolation of t representation. Upward deviations in the t-plots are due to adsorption and condensation in wide diameter pores, ascribed to mesoporous solids.

Values of the specific surface areas of the samples, as determined following the BET method [22] are included in Table 1. The specific surface area (S_{BET}) decreases sharply when SiO_2 (219 m^2 g^{-1}) is impregnated with 27 wt.% of CaO (Table 1). This can be explained considering that the binary support undergoes structural changes with the addition of CaO and the formation of CaO, $CaCO_3$ and/or Ca_2SiO_4 is suggested by XRD.

However, the S_{BET} specific surfaces remain almost unchanged in the calcined and reduced catalysts in which the binary support was impregnated with 0.36 or 0.6 wt.% rhodium using $RhCl_3 \cdot 3H_2O$ or $[NH_4]_3[RhCl_6] \cdot 3H_2O$ as precursor salts (Table 1).

Particle sizes and metal-support interaction

The Rh particles and nanocrystalline structures in the reduced catalysts were characterized through TEM. In a previous work,

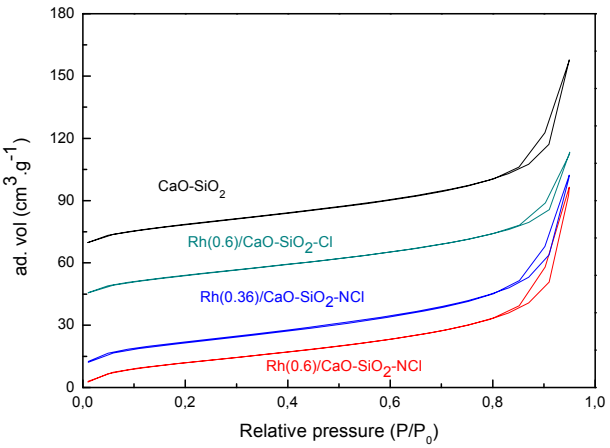

Fig. 1 – Adsorption–desorption isotherms of N_2 at 77 K of SiO_2, CaO–SiO_2 and Rh/CaO–SiO_2 catalysts.

Please cite this article in press as: Faroldi B, et al., Well-dispersed Rh nanoparticles with high activity for the dry reforming of methane, International Journal of Hydrogen Energy (2017), http://dx.doi.org/10.1016/j.ijhydene.2017.04.070

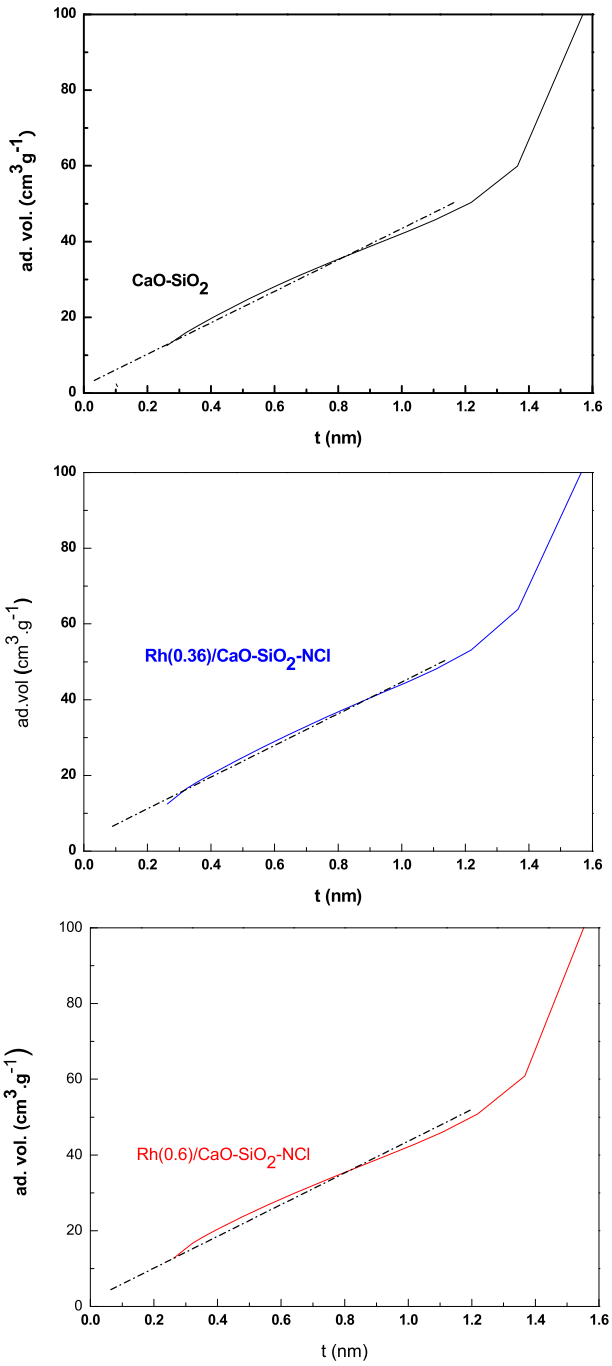

Fig. 2 – t-Plots for the adsorption of N_2 of CaO–SiO_2, Rh(0.36)/CaO–SiO_2–NCl and Rh(0.6)/CaO–SiO_2–NCl.

Table 1 – Specific surface areas of the calcined samples. S_{BET}, BET method, St, t-plot method.

Sample	S_{BET} (m^2g^{-1})	S_t (m^2g^{-1})
SiO_2	219	–
CaO–SiO_2	73	69
Rh(0.6)/CaO–SiO_2–Cl	65	66
Rh(0.6)/CaO–SiO_2–NCl	70	64
Rh(0.6)/CaO–SiO_2–NCl[a]	74	66
Rh(0.36)/CaO–SiO_2–NCl	67	65

[a] Reduced sample.

we studied the CaO(X)–SiO_2 binary supports with different CaO contents, 15, 20, 27 and 50 wt.% [18]. EDX mapping of oxygen, silicon and calcium revealed that CaO was uniformly distributed on SiO_2, in all the supports and Rh/CaO–SiO_2–Cl catalysts. Moreover, the Si/Ca atomic ratios were always close to the nominal values.

Histograms showing the metal particle size distribution for all the samples are displayed in Figs. 3–5 with representative TEM images of the catalyst as an inset. The Rh surface average particle sizes, calculated using Eq. (2) (Table 2), were between 1.4 nm and 1.7 nm. These particle sizes indicate that Rh is well dispersed on the catalyst surface and no agglomeration was observed in the TEM images.

The Rh dispersions measured after reduction at 823 K by CO chemisorption were 94 and 75% for the Rh(0.36) and Rh(0.6)/CaO–SiO_2–NCl catalysts, respectively. From these values, the metal particle sizes were calculated and are included in Table 2. Note that the average Rh particle sizes were coincident with the corresponding size measured from TEM images (Figs. 3–5) for all catalysts synthesized employing two different chloride-based salt precursors.

Force et al. [23], studied ceria-supported rhodium samples prepared from two different rhodium precursors (Rh (III) chloride and nitrate) to compare their behavior toward hydrogen reduction treatments. Results of FTIR and NMR techniques revealed that the presence of chloride ions delayed rhodium reduction and favored a higher dispersion of rhodium particles at the catalyst.

The characteristics of Rh surface species and their interaction with the binary support were investigated by CO adsorption followed by FTIR. Fig. 6 presents the spectra of the reduced Rh/CaO–SiO_2–NCl solids exposed at different CO pressures, where three main CO adsorbed features can be observed. The bands at about 2067 cm^{-1} are assigned to linearly adsorbed CO on metallic Rh (Rh^0–CO); the bands appearing at 2097 and 2030 cm^{-1} correspond to $Rh^+(CO)_2$ gem-dicarbonyls [24,25] and the broad features at about 1995 cm^{-1} are assigned to bridged-bonded CO [25,26].

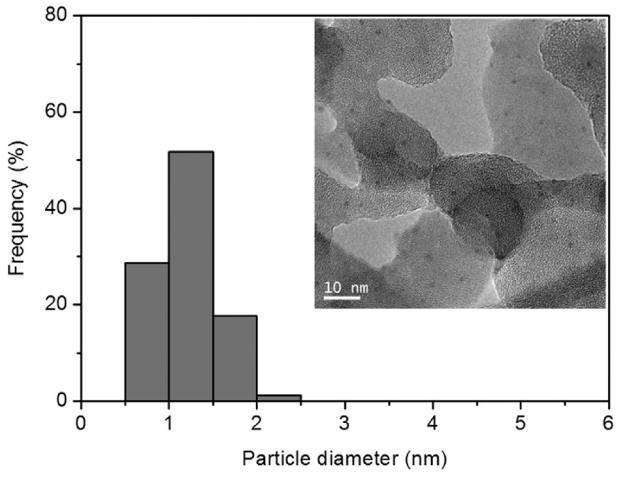

Fig. 3 – TEM image and metal particle distribution of Rh(0.36)/CaO–SiO_2–NCl (Surface average diameter = 1.4 nm). At least 150 particles were counted to obtain each distribution histogram.

Please cite this article in press as: Faroldi B, et al., Well-dispersed Rh nanoparticles with high activity for the dry reforming of methane, International Journal of Hydrogen Energy (2017), http://dx.doi.org/10.1016/j.ijhydene.2017.04.070

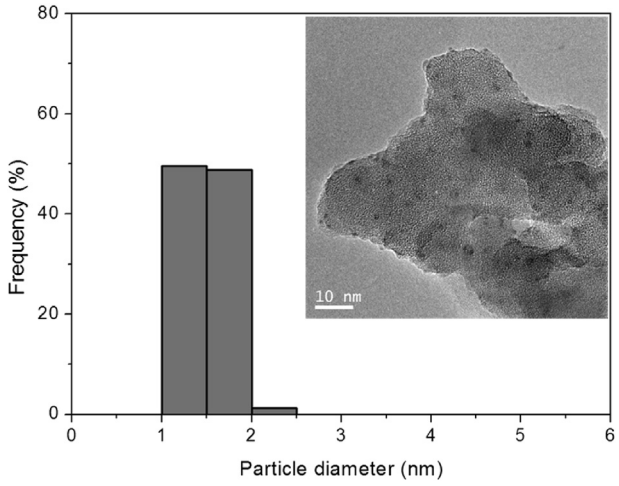

Fig. 4 – TEM image and metal particle distribution of Rh(0.6)/CaO–SiO_2–NCl (Surface average diameter = 1.6 nm). At least 150 particles were counted to obtain each distribution histogram.

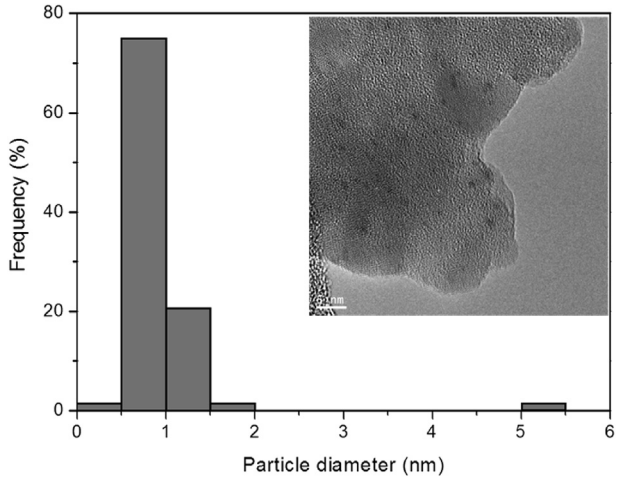

Fig. 5 – TEM image and metal particle distribution of Rh(0.6)/CaO–SiO_2–Cl (Surface average diameter = 1.7 nm). At least 150 particles were counted to obtain each distribution histogram.

In a previous work, we reported the spectrum of CO adsorbed at room temperature on Rh supported on SiO_2 [18]. The spectrum showed only two bands, one band at 2041 cm^{-1} corresponding to terminally bonded CO, and a broad band at 1916 cm^{-1} assigned to bridged-bonded CO. The dicarbonyl species were not observed on the Rh/SiO_2 catalyst, as previously reported by Dumesic and co-workers [24].

The modification of the silica support with CaO produced a shift to a higher wavenumber of linearly bonded CO bands (Fig. 6). A similar effect was reported by Knozinger and co-workers [27] after the addition of promoter oxides to Rh supported on SiO_2. The authors attributed this slight shift to a particle size effect due to the fact that the smaller particles present a higher fraction of edge and corner atoms, which are electron deficient. The effect of V, Nb and Ta oxides were also ascribed to the polarization of the small Rh clusters that electronically influences the stretching frequency of linearly bonded CO [27]. The band shift observed in our catalysts could be produced by both effects, taking into account their high Rh dispersion.

On Rh supported catalysts, the $Rh^+(CO)_2$ gem-dicarbonyls could be formed from highly dispersed metallic rhodium by an oxidation process involving isolated acidic OH groups of the support [27]. In our solids, the O–H wavenumbers of silanol groups were not modified by the adsorption of CO suggesting that Rh gem-dicarbonyls are placed directly on the promoter oxide and not on the silica oxygen. For ex-chloride Rh/CeO_2 samples, Force et al. [23] have considered that CO adsorption on the smaller particles can proceed by an oxidative rupture process of CO adsorbed, producing $Rh^+(CO)_2$, in which the Rh oxidation might be favored by the presence of chloride.

In order to correlate CO adsorption features with the surface properties of the catalyst, the FTIR spectra were decomposed in the characteristic bands of the adsorbed CO species (In Supplementary files, Fig. S2 shows the curve fitted spectrum for Rh/CaO–SiO_2–NCl solids) and their integrated intensities were determined to calculate the intensity ratios (Table 2). The signal intensities were normalized to the pellets weight to take into account the variation in the pellet thickness [27]. Note that the linear to gem-dicarbonyl (L/G) intensity ratio exhibits the lowest values for the Rh(0.36)/CaO–SiO_2–NCl catalyst, being the solid with the smallest particle size. The higher concentration of the $Rh^+(CO)_2$ gem-dicarbonyl species could be related to the small particle size that would favor the oxidation of these nanoparticles.

The spectra obtained for Rh catalysts after CO adsorption at 298 K and stepwise heating at 373, 473, 573 and 673 K are shown in Fig. 6A and B. Following the desorption steps, similar changes were observed in both catalysts. However, in the Rh(0.6) sample, the spectra variation was more appreciable. After evacuation at 298 K, the linear Rh–CO band decreases noticeably and shifts to a lower wavenumber indicating a lower density of adsorbed CO species which results in a weaker dipolar coupling. Both modifications (intensity and band position) increase when the temperature is increased and the Rh–CO signal disappears at about 573 K for Rh(0.6) and at 473 K for Rh(0.36) catalysts. At these temperatures, the signals assigned to $Rh^+(CO)_2$ gem-dicarbonyls are the only ones observed and disappear above 673 K for both catalysts.

Reaction rates for the dry reforming methane

In the last few years, there have been several reports focusing on the dry reforming of methane reaction with the purpose of producing synthesis gas at high temperatures (>873 K) [2,16,17]. However, few of them have studied this reaction at temperatures lower than 873 K [18,28,29]. When the aim is to produce ultrapure hydrogen using membrane reactors, low temperatures are required to operate this type of reactors [18]. Table 3 shows the catalytic results of the Rh(X)/CaO–SiO_2 solids, in comparison with those reported in the literature for Rh supported catalysts in this temperature range. Note that the reaction rates of the Rh(X)/CaO–SiO_2 catalyst were higher than those of the Rh and Ru catalysts supported on La_2O_3–SiO_2 [18,30]. In addition, Table 3 shows the turnover

Please cite this article in press as: Faroldi B, et al., Well-dispersed Rh nanoparticles with high activity for the dry reforming of methane, International Journal of Hydrogen Energy (2017), http://dx.doi.org/10.1016/j.ijhydene.2017.04.070

Table 2 – CO adsorption results, particles sizes and surface atomic concentration of reduced Rh catalysts.

Catalysts	L/B[d]		L/G[d]		Rh(%) (XPS)	D_{CO}[e] (%)	dp^{f}_{CO} (nm)	dp^{g}_{TEM} (nm)
	Adsorption ($P_{CO} = 1.3 \times 10^4$ Pa)	Desorption (298 K)	Adsorption ($P_{CO} = 1.3 \times 10^4$ Pa)	Desorption (298 K)				
Rh(0.36)/CaO–SiO_2–NCl[a]	6.5	3.6	2.2	1.6	0.14	94	1.2	1.4
Rh(0.6)/CaO–SiO_2–NCl[a]	14.0	6.7	3.7	2.6	0.30	75	1.5	1.6
Rh(0.6)/CaO–SiO_2–Cl[b]	10.0	3.8	2.8	1.8	0.21	69	1.6	1.7
Rh(0.6)/La_2O_3–SiO_2–Cl[b,c]	13.8	–	5.6	–	0.18	79	1.4	1.3

[a] Precursor: $[NH_4]_3[RhCl_6]$ $3H_2O$.
[b] Precursor: $RhCl_3 \cdot 3H_2O$.
[c] From Ref. [7].
[d] From FTIR CO spectra, linearly (L), dicarbonyl (G) and bridge (B) bonded CO.
[e] Metal dispersion calculated from CO chemisorption.
[f] Rh particle size calculated using the equation $dp = \frac{6 \cdot \upsilon_m}{D \cdot a_m}$ (Eq. 1), $\upsilon_m = 13.78 \times 10^{-3}$ nm^3 for Rh, $a_m = 7.58 \times 10^{-2}$ nm^2 [20].
[g] Surface average metal particle size calculated from the micrographs $d = \frac{\sum n_i d_i^3}{\sum n_i d_i^2}$ (Eq. 2), n_i is the number of particles. The number of particles counted was at least 150 in all the cases.

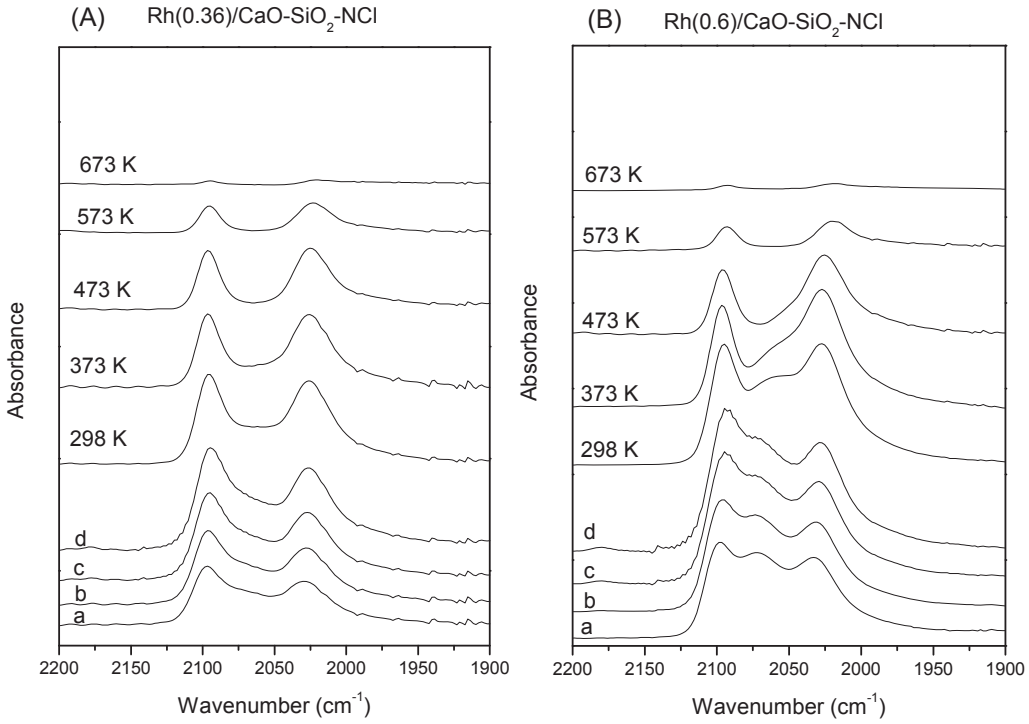

Fig. 6 – Thermal stability of the adsorbed CO species: FTIR spectra obtained from (A) Rh(0.36)/CaO–SiO_2–NCl and (B) Rh(0.6)/CaO–SiO_2–NCl catalysts reduced in hydrogen at 673 K following different CO adsorptions at 298 K, (a: $P_{CO} = 1.3 \times 10^2$ Pa, b: $P_{CO} = 1.3 \times 10^3$ Pa, c: $P_{CO} = 6.5 \times 10^3$ Pa and, d: $P_{CO} = 1.3 \times 10^4$ Pa). Also FTIR spectra obtained after stepwise heating under a dynamic vacuum at 298 K, 373 K, 473 K, 573 K and 673 K were included.

frequency values (TOF) calculated taking into account the Rh dispersion determined by CO chemisorption of the solids reduced at 823 K. It can be observed that the catalysts studied in this work present the higher activity per gram of catalyst and per mol of active site (TOF). Catalysts Pd(1.6%)/ZrO_2–La_2O_3 and Rh(0.8%)/CeO_2, evaluated in the dry reforming and steam reforming of methane respectively, exhibited an activity comparable with our catalysts.

An increase in CH_4 conversion with metal particle dispersion was reported by several authors [19,31,32]. Rh catalysts supported on CeO_2, $CeZrO_2$, ZrO_2 and SiO_2 were studied by Ligthart et al. [32] for steam methane reforming. The initial intrinsic surface atom reaction rate increased linearly with the Rh dispersion and it is not affected by the type of support. In agreement, Iglesia et al. [19] concluded that the methane turnover rates do not depend on the support of Rh catalysts. In a recent work, Yamaguchi and Iglesia [33] found similar turnover rates on Pd clusters on various supports (Al_2O_3, ZrO_2 and ZrO_2–La_2O_3) independently of Pd dispersion over a narrow range of 3.5–8.9%. They sustain that the supports with low reactivity for CO_2 activation can reverse the formation of carbon overlayers and inhibit deactivation, but do not

Please cite this article in press as: Faroldi B, et al., Well-dispersed Rh nanoparticles with high activity for the dry reforming of methane, International Journal of Hydrogen Energy (2017), http://dx.doi.org/10.1016/j.ijhydene.2017.04.070

Table 3 – Catalytic behavior of noble metal based catalysts for the dry reforming of methane at low temperature.

Catalysts	D (%)	Temperature (K)	CH_4 reaction rate[a] (Mol g metal^{-1} h^{-1})	TOF (s^{-1})	Stability (h)	Carbon formation (g gcat^{-1})	Ref
Rh(0.36)/CaO–SiO_2–NCl	94	823	194	5.9	48	Non detected	This work
Rh(0.6)/CaO–SiO_2–NCl	75	823	121	5.1	48	Non detected	This work
Rh(0.6)/CaO–SiO_2–Cl	69	823	57	2.4	48	Non detected	[18]
Rh(0.6)/La_2O_3–SiO_2–Cl	79	823	45.3	1.6	72	Non detected	[7]
Ru(0.6)/La_2O_3–SiO_2	24	823	36	4.2	72	Non detected	[30]
Rh(0.4%)/Al_2O_3	37.2	873	54.6	4.2	0.3	Not reported	[19]
Pd(1.6%)/ZrO_2–La_2O_3	5.3	823	18	10	0.2	Not reported	[33]
Rh(0.8%)/CeO_2[b]	51	773	252	14.1	15	0.33	[32]

[a] CH_4 reaction rates measured after 1 h on stream. The values are reported at a ±95% confidence interval.
[b] Evaluated in the steam reforming of methane reaction.

contribute to steady-state catalytic reforming rates. In our case, the high activity of the catalysts could be related not only to the active site but also to the support used. The CaO and La_2O_3 binary SiO_2 support could affect the turnover rates on Rh nanoparticles due to their reactivity with CO_2.

In the proposed mechanism for lanthanum based catalysts, CO_2 rapidly reacts with La_2O_3 to generate oxycarbonate which then reacts slowly with carbon to produce CO [34,35]. A bifunctional mechanism has also been described for Ni/ZrO_2–La_2O_3 catalysts promoted with calcium oxide. In this case, methane is activated on the Ni particles while CO_2 interacts with the CaO to form carbonates which scavenge carbon at the Ni–O–Ca interphase, thus explaining the enhanced stability of these solids [36].

Fig. 7 shows the stability and H_2/CO ratio results for the studied solids. After the activity measurements, the catalysts were kept under reaction with methane and carbon dioxide conversions close to equilibrium values employing a high W/F value (2.67×10^{-5} g h ml^{-1}) during 48 h. To compare the catalyst stabilities, the W/F was decreased at 4.5×10^{-6} g h ml^{-1} just to measure the reaction rates (conversions were lower than 10% in all cases). Both catalysts were stable and selective to hydrogen. The catalyst with a lower content of Rh presented a higher CH_4 reaction rate, expressing the reaction rate per gram of catalyst. Note that in all cases the H_2/CO ratio was always less than unity, which is due to the simultaneous occurrence of the reverse water gas shift reaction (RWGS) and the dry reforming reaction [7,37]. On the other hand, regarding the use of non-noble metal catalysts, in the literature there are many reports that study Ni-based catalysts at high temperature (T ≥ 973 K). However, few of them report catalytic results at low temperatures (773–873 K) [28,38,39]. Rodemerck et al. [39] studied Ni catalysts supported on mixed ZnO/Al_2O_3 at 673 K. However, the authors reported high initial activity followed by deactivation. Coperet et al. [38] investigated Ni/SiO_2 catalysts with different particle sizes, which deactivated during the first few minutes of reaction.

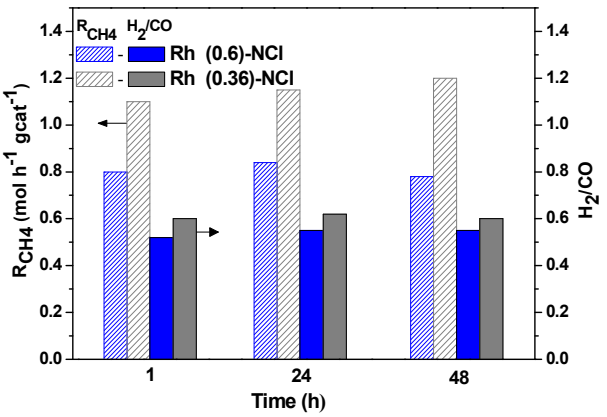

Fig. 7 – Stability tests for Rh/CaO–SiO_2–NCl catalysts carried out in the conventional fixed-bed reactor during 48 h.

A La–NiMgAlO catalyst, obtained by calcination of a hydrotalcite precursor, was evaluated in dry reforming of methane at different temperatures. At 973 K the catalyst showed no sign of deactivation during 200 h, however, when the temperature was decreased at 923 K, the methane and carbon dioxide conversions decreased from the beginning of the test [40].

Catalytic behavior in an integral reactor

The Rh(X)/CaO–SiO_2–NCl catalysts were evaluated for dry methane reforming without and with oxygen addition (CRM), using the same total flow that would be employed in the membrane reactor. Fig. 8 shows the methane and carbon dioxide conversions measured at different feed compositions. For both Rh catalysts, values close to equilibrium were achieved in DRM conditions, when CO_2/CH_4 was equal to 1. When this ratio was 1.9, the methane conversions increased although the equilibrium values could not be achieved, however the Rh(0.6) catalyst showed the highest value.

When oxygen was added to the reactant mixture, CH_4 conversions were higher than those obtained under the DRM conditions, whereas the CO_2 conversion decreased, in agreement with the equilibrium conversion values. In this case, the partial and the total oxidation of methane reactions might occur in parallel with the dry reforming and water gas shift reaction. The theoretical values (calculated employing UniSim software) could not be reached, the methane conversion being always lower than the equilibrium ones. This behavior could be due to the Rh re-oxidation that occurs when oxygen was added to the reactant mixture. Note that the presence of carbonaceous deposits in the used catalysts could not be detected through TGA.

Please cite this article in press as: Faroldi B, et al., Well-dispersed Rh nanoparticles with high activity for the dry reforming of methane, International Journal of Hydrogen Energy (2017), http://dx.doi.org/10.1016/j.ijhydene.2017.04.070

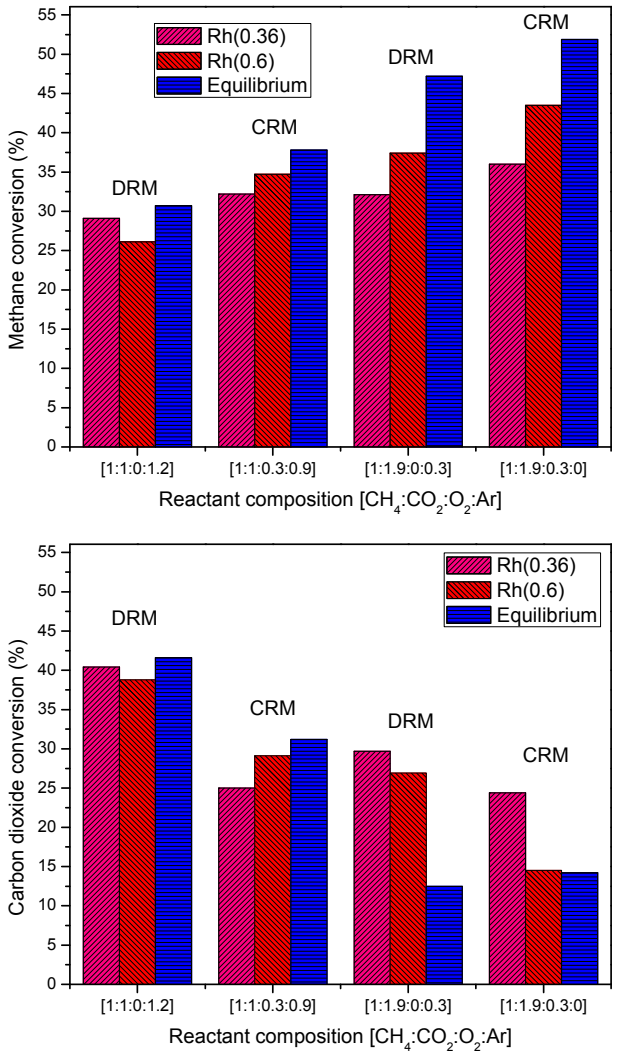

Fig. 8 – Catalytic behavior in an integral fixed-bed reactor for the dry reforming of methane with (CRM) and without oxygen addition (DRM). Catalyst mass = 0.2 g, W/F = 2 × 10^{-4} g h ml^{-1}, reaction temperature = 823 K. Equilibrium conversions were calculated using UniSim Design Software considering a Gibbs reactor [20].

Catalytic behavior in a membrane reactor

The more active and stable solids were evaluated in a membrane reactor. To compare the behavior of the catalyst-membrane system, we have defined a σ parameter considering variables (methane flow fed and sweep gas flow) that are directly related to the ability of the reactor to permeate hydrogen [6,9,41,42]. The methane flow fed is related to the space velocity and consequently to the catalyst ability to restore the equilibrium when hydrogen is removed from the reaction system.

Fig. 9 shows the effect of the σ parameter (Sweep gas ratio = Sweep gas flow rate/CH_4 flow fed) on methane conversion and hydrogen recovery. It can be observed that the methane conversions are higher than those of the equilibrium conversions in the sweep gas range studied for all catalysts. At lower sweep gas ratio, there is no significant difference in the conversion enhancement produced by both solids, Rh(X)/CaO–SiO_2–NCl (X = 0.36 and 0.6). When the sweep gas ratio increases, the conversion of the Rh (0.6) solid is higher, showing that the catalyst activity affects the performance of the membrane reactor.

However, when the sweep gas is higher than 50 ml min^{-1} ($\sigma \geq 9.6$), the conversion enhancement of Rh(0.36) is lower in comparison with the solid of higher metal load. The lower activity observed in the catalyst with low Rh content could be due to the partial deactivation of the catalyst, the membrane, or a combination of both. In either case, the activity loss could be due to an excessive carbon deposition, metal sintering and/or metal oxidation. The latter could be explained taking into account that for high values of sweep gas the hydrogen recovery increases, reducing the hydrogen partial pressure on the retentate side and increasing the CO_2 concentration [6]. For the solid prepared from $RhCl_3 \cdot 3H_2O$ precursor salt, a progressive increase of the conversion is observed with σ ratio.

Fig. 9 shows the hydrogen recovery as function of σ. For lower values of σ, the H_2 recovery is in agreement with the order of activity previously mentioned, while at higher values of σ it results in a lower hydrogen separation ratio for the more active catalyst with 0.36 wt.% of Rh. However, at higher values of σ, this membrane reactor (high selective membrane and active catalyst) was able to recover 80 percent of the hydrogen produced with high purity.

Some authors studied the dry reforming of methane employing membrane reactors. In an earlier work of dry reforming over a Pt (1.2 wt.%)/Al_2O_3 catalyst, we studied the effect of increasing the sweep gas flow rate using a porous mullite membrane [8]. We found a reasonable conversion enhancement and also a maximization of hydrogen selectivity because the progress of the secondary reverse water gas shift reaction is hindered as the sweep gas flow rate grows. Gallucci et al. [41] using Ni/Al_2O_3 as catalyst analyzed different operation variables such as temperature, pressure and reaction time. Using a dense Pd–Ag membrane, they found that the hydrogen recovery was only 25% at 723 K and a pressure of 2 × 10^5 Pa. The authors reported that the important carbon formation affects the stability of the catalyst and can also reduce the lifetime of the membrane. On the other hand, Oyama et al. [42] employing a Rh/Al_2O_3 catalyst coupled with a silica-based membrane studied the pressure effect on methane conversion and H_2 recovery in a pressure range of 100 kPa-2 MPa at 973 K. In the case of the dry methane reforming, the authors found that at pressures higher than 500 kPa, the hydrogen yield decreases since the reverse water gas shift reaction is favored. In a previous work [18], we reported the effect of pressure on methane conversion and hydrogen recovery in a range between 100 and 200 kPa in a dense Pd membrane reactor. An increase in the hydrogen recovery at pressure lower than 190 kPa was observed. The effect of pressure on the reactant conversion can be explained considering two opposite effects, a negative one owing to the thermodynamics of the reaction and a positive one related to the increase of hydrogen permeation through the dense palladium membrane.

In comparison with data reported in the literature, high values of conversion enhancement and H_2 recovery were

Please cite this article in press as: Faroldi B, et al., Well-dispersed Rh nanoparticles with high activity for the dry reforming of methane, International Journal of Hydrogen Energy (2017), http://dx.doi.org/10.1016/j.ijhydene.2017.04.070

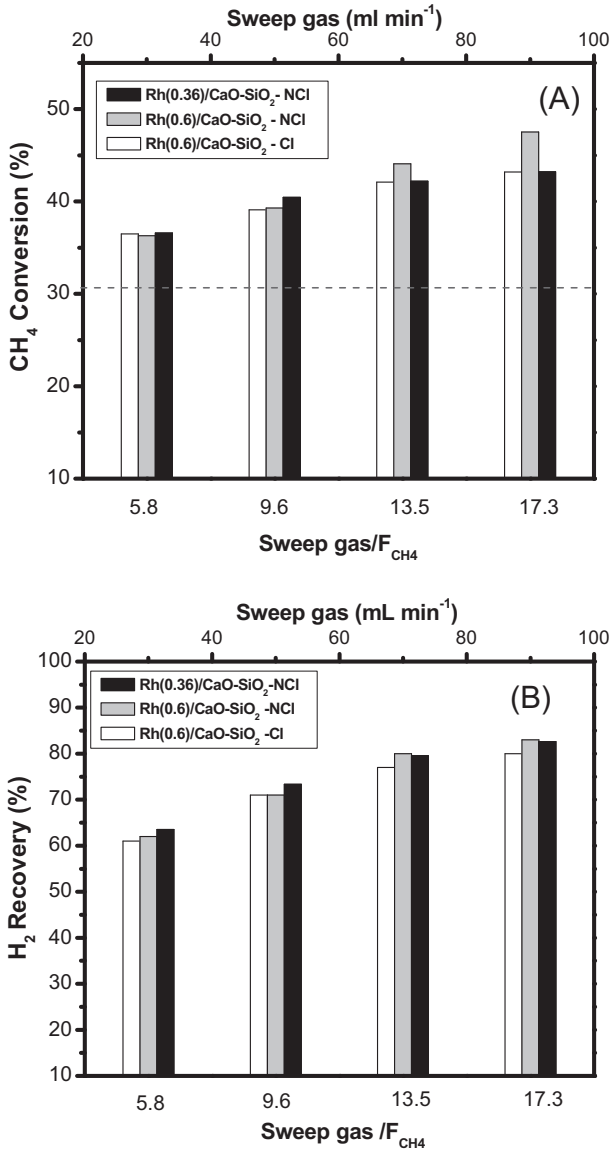

Fig. 9 – Effect of σ (sweep gas ratio = sweep gas flow rate/CH_4 flow fed) over methane conversion (A) and H_2 recovery (hydrogen permeated/hydrogen retentate ratio) (B) using a membrane reactor for Rh/CaO–SiO_2 catalysts. W/F: 1.5×10^{-3} g ml^{-1} h, membrane area: 8×10^{-4} m^2, T: 823 K, P: 101 kPa. The reactant mixture composition was CO_2:CH_4:Ar = 1:1:1.2. The dashed line represents the equilibrium value for CH_4 conversion.

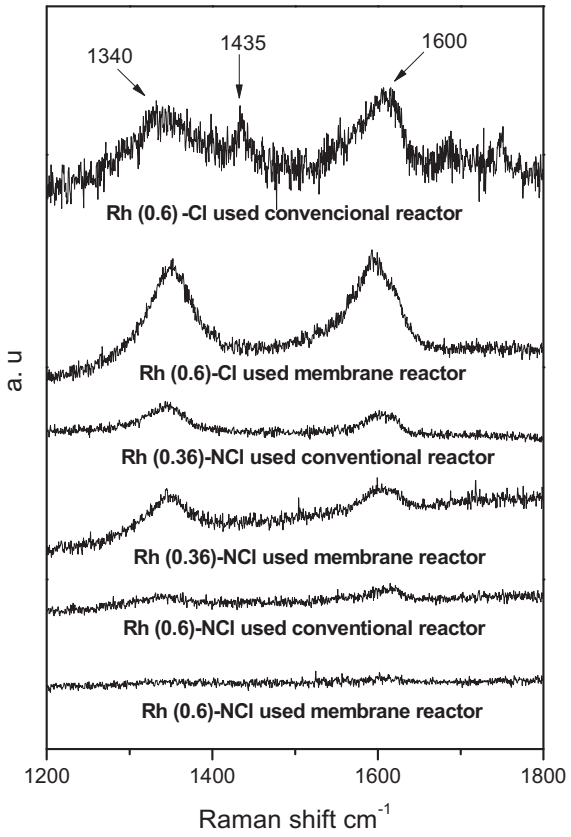

Fig. 10 – Laser Raman spectra of Rh/CaO–SiO_2 catalysts used in the integral fixed-bed and membrane reactors.

obtained in this work operating at 100 kPa and using a sweep gas flow to maintain the driving force between both sides of the membrane.

Carbon formation and surface oxidation states

In order to understand the different catalyst behavior at higher σ values, the solids used in the integral fixed-bed and membrane reactors were characterized by laser Raman spectroscopy, TEM and XPS. Fig. 10 shows the Raman spectra of the used catalysts in the region assigned to graphitic carbon (1200–1800 cm^{-1}). It can be observed that the solids prepared with the $[NH_4]_3[RhCl_6]\cdot 3H_2O$ precursor and evaluated in the membrane reactor present less intense bands corresponding to carbonaceous deposits (1340 and 1600 cm^{-1}) in comparison with the solids prepared with $RhCl_3\cdot 3H_2O$. However, all catalysts were stable for at least 48 h in the conventional fixed-bed reactor. In addition, through Thermogravimetric Analysis, it was not possible to quantify the carbon deposits, suggesting that the carbon content was below the detection limit (0.1 μg/mg of catalyst) of the TGA equipment. The formation of scarce carbon filaments of different sizes and length was also detected by TEM in the catalysts after being exposed 48 h on stream (Fig. S3). Therefore, these results suggest that the cause of the partial activity loss in the membrane reactor could not be related to carbon formation. No modifications in the texture of the CaO–SiO_2 were observed by TEM in the used catalysts. In addition, the distribution and the average Rh particle sizes (not shown) were similar to those obtained for the catalysts before reaction, suggesting that Rh particle sintering was not produced.

XPS analysis was performed on the catalysts after reduction at 823 K, in order to analyze variation on Rh surface concentration and oxidation states.

The XPS fractional concentrations are given in Table 4 for the Rh(X)/CaO–SiO_2–NCl solids reduced in situ. The C1s, O1s, Si 2p, Ca 2p and Rh 3d spectra were analyzed and no significant changes in binding energies (BEs) were observed between the different samples. For both reduced solids, the C1s spectra

Please cite this article in press as: Faroldi B, et al., Well-dispersed Rh nanoparticles with high activity for the dry reforming of methane, International Journal of Hydrogen Energy (2017), http://dx.doi.org/10.1016/j.ijhydene.2017.04.070

Table 4 – XPS fractional atomic concentrations for the reduced and used Rh/CaO–SiO_2–NCl catalysts.[a]

Catalysts	Rh	Ca	Si	O_{532}[b]	O_{530}[c]	C_{283}/Si	O_{532}/Si	$CO_3^{=}$/Si
Rh(0.36) reduced	0.0015	0.09	0.40	0.45	0.07	0.37	1.10	0.01
Rh(0.6) reduced	0.0032	0.08	0.40	0.45	0.07	0.27	1.10	0.01
Rh(0.36) used IR[d]	0.0023 (26/74)[e]	0.04	0.33	0.60	0.02	0.08	1.81	0.02
Rh(0.6) used IR[d]	0.0022 (41/59)[e]	0.04	0.33	0.61	0.02	0.10	1.85	0.03
Rh(0.36) used MR	0.0020 (0/100)[e]	0.06	0.29	0.55	0.10	1.13	1.90	0.01
Rh(0.6) used MR	0.0022 (22/78)[e]	0.02	0.32	0.62	0.03	0.88	1.90	0.02

[a] Calculated considering Rh, Ca, Si and O.
[b] O atomic concentration for the BE peak at 532 eV.
[c] O atomic concentration for the BE peak at 530 eV.
[d] Used in an integral reactor.
[e] Surface Rh^0/Rh^{n+} intensity ratio determined through curve fitting of Rd 3d spectrum (Fig. 10).

show two main peaks at 284.6 and 289.2–288.3 eV. The low BE peak corresponds to the C–H carbon (taken as binding energy reference) while the very low intensity peak at 289–288.3 eV was assigned to carbon from $CO_3^{=}$ species [43].

The spectra of O1s from the reduced samples show a main peak that appears at 532.0 ± 0.1 eV and could be attributed to Si–O bonds. One additional peak located at the low BE side (530 ± 0.1 eV) with lower intensity has to be considered (Fig. S4). This peak is attributed to Ca–O bonds. Note that for bulk crystalline $CaCO_3$, a main peak, symmetric and sharp, whose given BE is about 531.2 eV, was assigned to the O bonds in a $CO_3^{=}$ species [43].

The Ca $2p_{3/2}$ core level spectrum from the reduced samples shows a binding energy of 347 ± 0.1 eV, which was attributable to CaO (BE = 347.1 eV) [18,44], although the presence of $CaCO_3$ and Ca_2SiO_4 could not be ruled out (BE = 346.9 eV) [43]. Note that the surface CO_3^{2-}/Si ratio (0.01) is very low in comparison with the Ca/Si surface ratio (varying between 0.2 and 0.22). The concentration of the O species at 530.1 eV presents similar values with respect to Ca concentration, with a Ca/O_{530} ratio near 1, even in the catalysts after 48 h on stream. Similar results were discussed in a previous publication [18] and were assigned to Ca–O bonds, suggesting that CaO is evenly distributed on the amorphous SiO_2.

Fig. 11 shows Rh 3d XPS spectra from Rh(0.36) and Rh(0.6) reduced at 673 K in situ and used at conversions near thermodynamic equilibrium on the integral fixed-bed or membrane reactor.

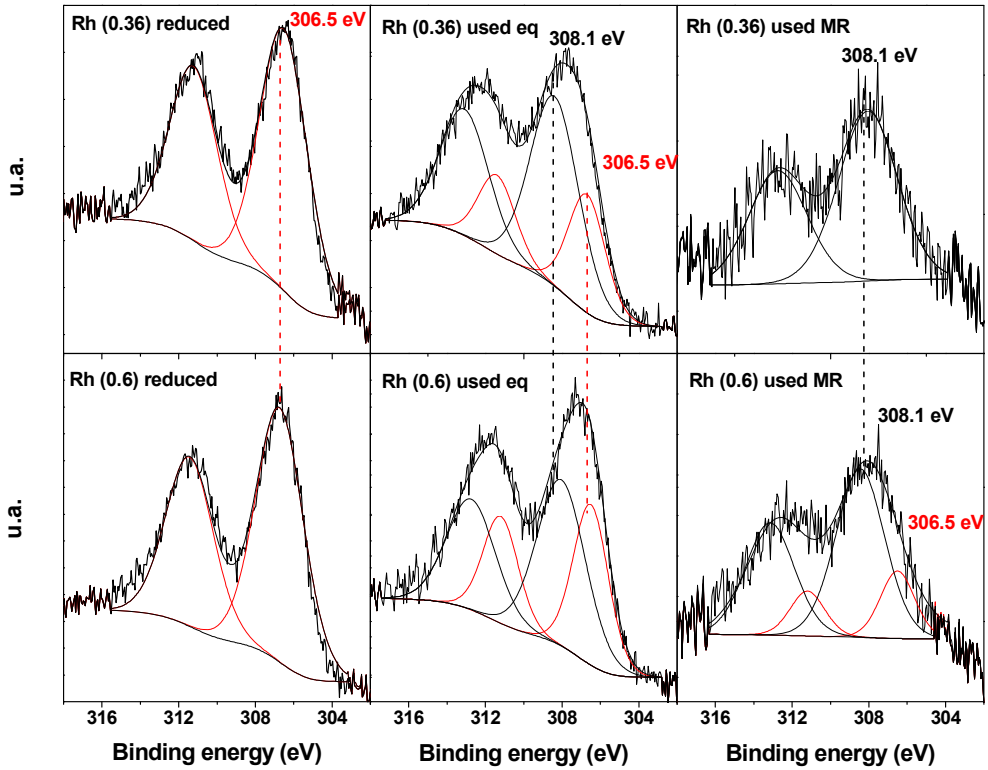

Fig. 11 – Rh 3d XPS spectra from Rh(0.36) and Rh(0.6)–NCl catalysts in situ reduced at 673 K and used under equilibrium in the integral and membrane reactors. The labeled Rh $3d_{5/2}$ peaks correspond to metallic rhodium at 306.5 eV and oxidized Rh^{n+} at 308.1 eV.

Please cite this article in press as: Faroldi B, et al., Well-dispersed Rh nanoparticles with high activity for the dry reforming of methane, International Journal of Hydrogen Energy (2017), http://dx.doi.org/10.1016/j.ijhydene.2017.04.070

The XPS Rh 3d spectra of reduced solids show a signal at 306.5 eV assigned to metallic rhodium. However, the solids used in an integral reactor also present another stronger signal at 308.1 eV assigned to oxidized Rh^{n+}. In the spectrum of the used Rh(0.36) solid in the membrane reactor only the signal at 308.1 eV is observed, indicating the complete oxidation of Rh in the near-surface region analyzed by the XPS technique. In the case of Rh(0.6) solid used under the same conditions, both Rh species are present (Table 4). XPS data for Rh(0.6)/CaO–SiO_2–Cl were previously reported by Múnera et al. [18]. For this solid, the complete reduction to Rh^0 was detected with a Rh $3d_{5/2}$ binding energy of 306.9 eV for both, the reduced and the used solid in the integral reactor.

Analyzing the outlet gas concentrations in both reactor types (integral and membrane reactor), we could observe that in the case of the membrane reactor the hydrogen molar concentration in the reaction side is decreased from 10 to 3–5% when the sweep gas ratio increased from 0 to 17.3, while the CO_2 concentration is changed between 18 and 15%. These values suggest that the reaction atmosphere would be more oxidant in the membrane reactor. As a consequence, the oxidation of Rh surface species would be favored. In the case of the catalyst with lower metal loading and lower Rh particle size, the surface Rh species was completely oxidized, being the main cause of the activity loss at higher σ values in the membrane reactor.

Ligthart et al. [32] studied catalysts with Rh nanoparticles between 2 and 9 nm and found that Rh particles smaller than 2.5 nm deactivate more strongly than catalysts with larger nanoparticles under the steam reforming conditions. Through the characterization of used catalysts by X-ray absorption spectroscopy, they observed an increase in the fraction of oxidic Rh as well as an increase in the Rh–O coordination shell for the catalysts with very small Rh particles. Thus, the oxidation of very small Rh particles was proposed as the explanation for catalyst deactivation.

In our catalysts, no correlation was found with the presence of very low amounts of carbon deposits (Fig. 10). Besides, no agglomeration of the Rh nanoparticles was observed through TEM characterization. These results suggest that the main cause for the decrease in the activity of highly dispersed Rh/CaO–SiO_2–NCl catalysts is the oxidation of the small Rh nanoparticles.

Conclusions

Low loading Rh catalysts supported on CaO–SiO_2 with metal particle sizes of about 1.4–1.7 nm were prepared employing different precursor salts. This particle size range indicates that Rh is well dispersed on the catalyst surface and that no agglomeration exists.

For all solids, a high stability was observed after 48 h on stream for the dry reforming of methane. In addition, all solids presented a high methane reaction rate, Rh(0.36)/CaO–SiO_2–NCl being the most active and well-dispersed catalyst. As a consequence, they were selected for their application in a membrane reactor under different conditions.

In the membrane reactor, the methane conversions were higher than the equilibrium conversions for the sweep gas range employed for all catalysts.

At lower sweep gas ratios, no significant difference was observed in the conversion enhancement obtained with both solids. However, when the sweep gas ratio increased, the conversion of the Rh(0.36) solid was lower suggesting that the partial deactivation of the catalyst has occurred. In order to understand the different catalyst behavior at higher sweep gas/methane fed ratios, the solids used in the integral fixed-bed and membrane reactors were characterized by laser Raman spectroscopy, TEM and XPS.

The formation of scarce carbon filaments without modification of Rh particle sizes was observed by TEM in the catalysts after being exposed 48 h on stream. In addition, it was not possible to quantify the carbon deposits through TGA, indicating that the partial activity loss in the membrane reactor could not be related to carbon formation. However, surface re-oxidation was detected through XPS measurements, suggesting that the main cause for the decrease in the activity of the highly dispersed Rh(0.36)/CaO–SiO_2 catalyst could be the oxidation of small Rh nanoparticles.

Acknowledgments

The authors wish to acknowledge the financial support received from ANPCyT 2014-1948, UNL and CONICET and from the Spanish Government under projects CTQ2011-29272-C04-01. Thanks are also given to ANPCyT for Grant PME 8 – 2003 to finance the purchase of the UHV Multi Analysis System and to Fernanda Mori for her help in the XPS measurements.

Appendix A. Supplementary data

Supplementary data related to this article can be found at http://dx.doi.org/10.1016/j.ijhydene.2017.04.070.

REFERENCES

[1] Vannice MA, Bradford MCJ. CO_2 reforming of CH_4. Catal Rev Sci Eng 1999;41:1–42.
[2] Pakhare D, Spivey J. A review of dry (CO_2) reforming of methane over noble metal catalysts. Chem Soc Rev 2014;43:7813–37.
[3] Shi C, Zhang SH, Li XS, Zhang AJ, Shi M, Zhu YJ, et al. Synergism in NiMoOx precursors essential for CH_4/CO_2 dry reforming. Catal Today 2014;233:46–52.
[4] Wang N, Shen K, Yu XP, Qian WZ, Chu W. Preparation and characterization of a plasma treated NiMgSBA-15 catalyst for methane reforming with CO_2 to produce syngas. Catal Sci Technol 2013;3:2278–87.
[5] Munera JF, Carrara C, Cornaglia LM, Lombardo EA. Combined oxidation and reforming of methane to produce pure H_2 in a membrane reactor. Chem Eng J 2010;161:204–11.
[6] Faroldi B, Carrara C, Lombardo E, Cornaglia L. Production of ultrapure hydrogen in a Pd-Ag membrane reactor using Ru/La_2O_3 catalysts. Appl Catal A Gen 2007;319:38–46.

[7] Irusta S, Múnera J, Carrara C, Lombardo EA, Cornaglia LM. A stable, novel catalyst improves hydrogen production. Appl Catal A Gen 2005;287:147–58.
[8] Ferreira-Aparicio P, Rodríguez-Ramos I, Guerrero-Ruiz A. On the applicability of membrane technology to the catalyzed dry reforming of methane. Appl Catal A Gen 2002;237:239–52.
[9] Abu El Hawa H, Lundin S-T, Patki N, Douglas Way J. Steam methane reforming in a Pd-Au membrane reactor: long-term assessment. Int J Hydrogen Energy 2016;41:10193–201.
[10] Gallucci F, Fernandez E, Corengia P, van Sint Annaland M. Recent advances on membranes and membrane reactors for hydrogen production. Chem Eng Sci 2013;92:40–66.
[11] Boeltken T, Wunsch A, Gietzelt T, Pfeifer P, Dittmeyer R. Ultra-compact microstructured methane steam reformer with integrated Palladium membrane for on-site production of pure hydrogen: experimental demonstration. Int J Hydrogen Energy 2014;39:18058–68.
[12] Gallucci F, van Sintannaland M, Kuipers JAM. Theoretical comparison of packed bed and fluidized bed membrane reactors for methane reforming. Int J Hydrogen Energy 2010;35:7142–50.
[13] Da Silva AM, Mattos LV, Múnera J, Lombardo E, Noronha FB, Cornaglia L. Study of the performance of Rh/La_2O_3-SiO_2 and Rh/CeO_2 catalysts for SR of ethanol in a conventional fixed-bed reactor and a membrane reactor. Int J Hydrogen Energy 2015;40:4154–66.
[14] Ross RH. Natural gas reforming and CO_2 mitigation. Catal Today 2005;100:151–8.
[15] Hu YH, Ruckenstein E. Catalytic conversion of methane to synthesis gas by partial oxidation and CO_2 reforming. Adv Catal 2004;48:297–345.
[16] Duan Y, Shang R, Zhong X, Xie W, Wang X, Huang L. In-situ synthesis of Ni single bond Mo_2C/Al_2O_3 catalysts for dry reforming of methane. Int J Hydrogen Energy 2016;41–47:21955–64.
[17] Gamba O, Moreno S, Molina R. Catalytic performance of Ni–Pr supported on delaminated clay in the dry reforming of methane. Int J Hydrogen Energy 2011;36–2:1540–50.
[18] Múnera J, Faroldi B, Frutis E, Lombardo EA, Cornaglia L, González Carrazán S. Supported Rh nanoparticles on $CaO–SiO_2$ binary systems for the reforming of methane by carbon dioxide in membrane reactors. Appl Catal A Gen 2014;474:114–24.
[19] Wei J, Iglesia E. Structural requirements and reaction pathways in methane activation and chemical conversion catalyzed by rhodium. J Catal 2004;225:116–27.
[20] Faroldi B, Bosko ML, Munera J, Lombardo E, Cornaglia L. Comparison of $Ru/La_2O_2CO_3$ performance in two different membrane reactors for hydrogen production. Catal Today 2013;213:135–44.
[21] Brunauer S, Emmett PH, Teller E. Adsorption of gases in multimolecular layers. J Am Chem Soc 1938;60:309–19.
[22] Sing KSW, Everett DH, Haul RAW, Moscou L, Pierotti RA, Rouquerol J, et al. Reporting physisorption data for gas/solid systems with special reference to the determination of surface area and porosity. Pure Appl Chem 1985;57:603–19.
[23] Force C, Belzunegui JP, Sanz J, Martínez-Ariasand A, Soria J. Influence of precursor salt on metal particle formation in Rh/CeO_2 catalysts. J Catal 2001;197:192–9.
[24] He R, Kusaka H, Mavrikakis M, Dumesic JA. Microcalorimetric, infrared spectroscopic and DFT studies of CO adsorption on Rh and Rh-Te catalysts. J Catal 2003;217:209–21.
[25] Basu S, Panayotov D, Yates JT. Rhodium-carbon monoxide surface chemistry: the involvement of surface hydroxyl groups on alumina and silica supports. J Am Chem Soc 1988;110:2074–81.
[26] Bernal S, Blanco G, Calvino J, Rodriguez-Izquierdo M, Vidal H. Influence of the preparation procedure on the chemical and microstructural properties of lanthana promoted Rh/SiO_2 catalysts: a FTIR spectroscopic study of chemisorbed CO. J Alloys Compd 1997;250:461–6.
[27] Beutel T, Alekseev O, Rydin Y, Likholobov V, Knozinger H. FTIR spectroscopic study and CO hydrogenation on V, Nb, and Ta oxide promoted Rh/SiO_2 catalysts. J Catal 1997;169:132–42.
[28] Dębek R, Galvez ME, Launay F, Motak M, Grzybek T, Da Costa O. Low temperature dry methane reforming over Ce, Zr and CeZr promoted Ni–Mg–Al hydrotalcite-derived catalysts. Int J Hydrogen Energy 2016;41:11616–23.
[29] Elsayed NH, RobertsN RM, Joseph B, Kuhn JN. Low temperature dry reforming of methane over Pt-Ni-Mg/ceria-zirconia catalysts. Appl Catal B Env 2015;179:213–9.
[30] Faroldi BM, Lombardo EA, Cornaglia LM. Surface properties and catalytic behavior of Ru supported on composite $La_2O_3–SiO_2$ oxides. Appl Catal A Gen 2009;369:15–26.
[31] Jones G, Jakobsen JG, Shim SS, Kleis J, Andersson MP, Rossmeisl J, et al. First principles calculations and experimental insight into methane steam reforming over transition metal catalysts. J Catal 2008;259:147–60.
[32] Ligthart DAJM, van Santen RA, Hensen EJM. Influence of particle size on the activity and stability in steam methane reforming of supported Rh nanoparticles. J Catal 2011;280:206–20.
[33] Yamaguchi A, Iglesia E. Catalytic activation and reforming of methane on supported palladium clusters. J Catal 2010;274:52–63.
[34] Múnera JF, Irusta S, Cornaglia LM, Lombardo EA, Vargas Cesar D, Schmal M. Kinetics and reaction pathway of the CO_2 reforming of methane on Rh supported on lanthanum-based. J Catal 2007;245:25–34.
[35] Verykios XE. Catalytic dry reforming of natural gas for the production of chemicals and hydrogen. Int J Hydrogen Energy 2003;28:1045–63.
[36] Bachiller-Baeza B, Mateos-Pedrero C, Soria MA, Guerrero-Ruiz A, Rodemerck U, Rodríguez-Ramos I. Transient studies of low-temperature dry reforming of methane over Ni-CaO/ZrO_2-La_2O_3. Appl Catal B Env 2013;129:450–9.
[37] Soria MA, Mateos-Pedrero C, Guerrero-Ruiz A, Rodríguez-Ramos I. Thermodynamic and experimental study of combined dry and steam reforming of methane on Ru/ZrO_2-La_2O_3 catalyst at low temperature. Int J Hydrogen Energy 2011;36:15212–20.
[38] Baudouin D, Rodemerck U, Krumeich F, Mallmann A, Szeto K, Ménard H, et al. Particle size effect in the low temperature reforming of methane by carbon dioxide on silica-supported Ni nanoparticles. J Catal 2013;297:27–34.
[39] Sokolov S, Radnik J, Schneider M, Rodemerck U. Low-temperature CO_2 reforming of methane over Ni supported on ZnAl mixed metal oxides. Int J Hydrogen Energy 2017;42:9831–9.
[40] Serrano-Lotina A, Daza L. Long-term stability test of Ni-based catalyst in carbon dioxide reforming of methane. Appl Catal A General 2014;474:107–13.
[41] Gallucci F, Tosti S, Basile A. Pd–Ag tubular membrane reactors for methane dry reforming: a reactive method for CO_2 consumption and H_2 production. J Membr Sci 2008;317:96–105.
[42] Oyama ST, Hacarlioglu P, Gu Y, Lee D. Dry reforming of methane has no future for hydrogen production: comparison with steam reforming at high pressure in standard and membrane reactors. Int J Hydrogen Energy 2012;37:10444–50.
[43] Kiehl J, Ben-Azzouz C, Dentel D, Derivaz M, Bischoff JL, Delaite C, et al. Grafting process of ethyl trimethoxysilane and polyphosphoric acid on calcium carbonate surface. Appl Surf Sci 2013;264:864–71.
[44] Blanchard DL, Baer DR. The interactions of Co, Mn and water with calcite surfaces. Surf Sci 1992;276:27–39.

Please cite this article in press as: Faroldi B, et al., Well-dispersed Rh nanoparticles with high activity for the dry reforming of methane, International Journal of Hydrogen Energy (2017), http://dx.doi.org/10.1016/j.ijhydene.2017.04.070